

# Multi-scale discrete approximations of Fourier integral operators associated with canonical transformations and caustics <sup>\*</sup>

Maarten V. de Hoop<sup>†</sup>   Gunther Uhlmann<sup>‡</sup>   András Vasy<sup>§</sup>   Herwig Wendt<sup>¶</sup>

May 9, 2022

## Abstract

We develop an algorithm for the computation of general Fourier integral operators associated with canonical graphs. The algorithm is based on dyadic parabolic decomposition using wave packets and enables the discrete approximate evaluation of the action of such operators on data in the presence of caustics. The procedure consists in the construction of a universal operator representation through the introduction of locally singularity-resolving diffeomorphisms, enabling the application of wave packet driven computation, and in the construction of the associated pseudo-differential joint-partition of unity on the canonical graphs. We apply the method to a parametrix of the wave equation in the vicinity of a cusp singularity.

## 1 Introduction

In this paper, we develop an algorithm for applying Fourier integral operators associated with canonical graphs using wave packets. To arrive at such an algorithm, we construct a universal oscillatory integral representation of the kernels of these Fourier integral operators by introducing singularity resolving diffeomorphisms where caustics occur. The universal representation is of the form such that the algorithm based on the dyadic parabolic decomposition of phase space previously developed by the authors applies [2]. We refer to [7, 8, 10, 11] for related computational methods aiming at the evaluation of the action of Fourier integral operators.

The algorithm comprises a geometrical component, bringing the local representations in universal form, and a wave packet component which yields the application of the local operators. Here, we develop the geometrical component, which consists of the following steps. First we determine the location of caustics on the canonical relation of the Fourier integral operator. For each point on a caustic we determine the associated specific rank deficiency and construct an appropriate diffeomorphism, resolving the caustic in open neighborhoods of this point. We determine the (local) phase function of the composition of the Fourier integral operator and the inverse of the diffeomorphism in terms of universal coordinates and detect the largest set on which it is defined. We evaluate the preimage of this set on the canonical relation. We continue this procedure until the caustic is covered with overlapping sets, associated with diffeomorphisms for the

---

<sup>\*</sup>The first three authors were partially supported by the National Science Foundation under grant CMG-1025259 and are grateful for the stimulating environment at the MSRI in Berkeley where this research was initiated in the Fall 2010.

<sup>†</sup>Department of Mathematics, Purdue University, West Lafayette, IN (mdehoop@math.purdue.edu)

<sup>‡</sup>Department of Mathematics, University of Washington, Seattle, WA, and Department of Mathematics, UC Irvine, Irvine, CA (gunther@math.washington.edu)

<sup>§</sup>Department of Mathematics, Stanford University, Stanford, CA (andras@math.stanford.edu)

<sup>¶</sup>Department of Mathematics, Purdue University, West Lafayette, IN; now at IRIT, CNRS, University of Toulouse, France (herwig.wendt@irit.fr)

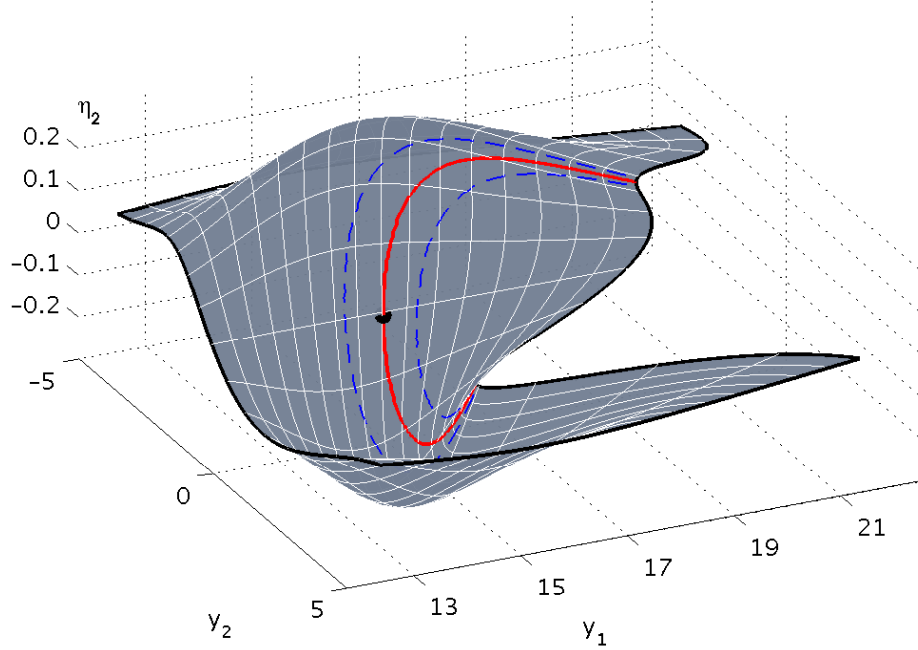


Figure 1: Projection  $\bar{\Lambda}(y, \eta_2)$  of a slice  $\xi = \xi_0$  of the canonical relation  $\Lambda$  associated with a half-wave equation in the vicinity of a caustic (red solid line, the blue dashed lines indicate the neighborhood of the singularity) caused by a low velocity lens. The white solid lines are connected to a regular grid in  $x$  by bicharacteristics. The black dot indicates the center of an open neighborhood of conjugate points  $(x_0, \xi_0) \mapsto (y_0, \eta_0)$  for which the projection onto standard microlocal focal coordinates  $(y, \xi)$  is not diffeomorphic.

corresponding rank deficiencies. Then we repeat the steps for each caustic and arrive at a collection of open sets covering the canonical relation.

The complexity of the algorithm for general Fourier integral operators as compared to the non-caustic case arises from switching, in the sets covering a small neighborhood of the caustics, from a global to a local algorithm using a pseudodifferential partition of unity.

As an application we present the computation of a parametriz of the wave equation in a heterogeneous, isotropic setting for long-time stepping in the presence of caustics.

## Curvelets, wave packets

We briefly discuss the (co)frame of curvelets and wave packets [9, 13, 24]. Let  $u \in L^2(\mathbb{R}^n)$  and consider its Fourier transform,  $\hat{u}(\xi) = \int u(x) \exp[-i\langle x, \xi \rangle] dx$ .

One begins with an overlapping covering of the positive  $\xi_1$  axis ( $\xi' = \xi_1$ ) by boxes of the form

$$B_k = \left[ \xi'_k - \frac{L'_k}{2}, \xi'_k + \frac{L'_k}{2} \right] \times \left[ -\frac{L''_k}{2}, \frac{L''_k}{2} \right]^{n-1}, \quad (1)$$

where the centers  $\xi'_k$ , as well as the side lengths  $L'_k$  and  $L''_k$ , satisfy the parabolic scaling condition

$$\xi'_k \sim 2^k, \quad L'_k \sim 2^k, \quad L''_k \sim 2^{k/2}, \quad \text{as } k \rightarrow \infty.$$

Next, for each  $k \geq 1$ , let  $\nu$  vary over a set of  $\sim 2^{k(n-1)/2}$  uniformly distributed unit vectors. Let  $\Theta_{\nu, k}$  denote a choice of rotation matrix which maps  $\nu$  to  $e_1$ , and  $B_{\nu, k} = \Theta_{\nu, k}^{-1} B_k$ . In the (co-)frame construction, one encounters two sequences of smooth functions on  $\mathbb{R}^n$ ,  $\hat{\chi}_{\nu, k}$  and  $\hat{\beta}_{\nu, k}$ , each supported in  $B_{\nu, k}$ , so that they

form a co-partition of unity,  $\hat{\chi}_0(\xi)\hat{\beta}_0(\xi) + \sum_{k \geq 1} \sum_{\nu} \hat{\chi}_{\nu,k}(\xi)\hat{\beta}_{\nu,k}(\xi) = 1$ , and satisfy the estimates

$$|\langle \nu, \partial_{\xi} \rangle^j \partial_{\xi}^{\alpha} \hat{\chi}_{\nu,k}(\xi)| + |\langle \nu, \partial_{\xi} \rangle^j \partial_{\xi}^{\alpha} \hat{\beta}_{\nu,k}(\xi)| \leq C_{j,\alpha} 2^{-k(j+|\alpha|/2)}.$$

One then forms  $\hat{\psi}_{\nu,k}(\xi) = \rho_k^{-1/2} \hat{\beta}_{\nu,k}(\xi)$ ,  $\hat{\varphi}_{\nu,k}(\xi) = \rho_k^{-1/2} \hat{\chi}_{\nu,k}(\xi)$ , with  $\rho_k = \text{vol}(B_k)$ , satisfying the estimates

$$\forall N : \left. \begin{array}{l} |\varphi_{\nu,k}(x)| \\ |\psi_{\nu,k}(x)| \end{array} \right\} \leq C_N 2^{k(n+1)/4} (2^k |\langle \nu, x \rangle| + 2^{k/2} \|x\|)^{-N}. \quad (2)$$

To obtain a (co)frame, one introduces the integer lattice:  $X_j := (j_1, \dots, j_n) \in \mathbb{Z}^n$ , the dilation matrix  $D_k = \frac{1}{2\pi} \begin{pmatrix} L'_k & 0_{1 \times n-1} \\ 0_{n-1 \times 1} & L''_k I_{n-1} \end{pmatrix}$ ,  $\det D_k = (2\pi)^{-n} \rho_k$ , and points  $x_j^{\nu,k} = \Theta_{\nu,k}^{-1} D_k^{-1} X_j$ . The frame elements ( $k \geq 1$ ) are then defined in the Fourier domain as  $\hat{\varphi}_{\gamma}(\xi) = \hat{\varphi}_{\nu,k}(\xi) \exp[-i \langle x_j^{\nu,k}, \xi \rangle]$ ,  $\gamma = (x_j^{\nu,k}, \nu, k)$ , and similarly for  $\hat{\psi}_{\gamma}(\xi)$ . The function  $\varphi_{\nu,k}$  is referred to as a wave packet. One obtains the transform pair

$$u_{\gamma} = \int u(x) \overline{\psi_{\gamma}(x)} dx, \quad u(x) = \sum_{\gamma} u_{\gamma} \varphi_{\gamma}(x). \quad (3)$$

## 2 Fourier integral operators and caustics

We consider Fourier integral operators,  $F$ , associated with canonical graphs. We allow the formation of caustics.

### 2.1 Oscillatory integrals, local coordinates

Let  $(y, x_{I_i}, \xi_{J_i})$  be local coordinates on the canonical relation,  $\Lambda$  say, of  $F$ , and  $S_i$  a corresponding generating function: If, at a point on  $\Lambda$ ,  $(dy, dx_I)$  are linearly independent and  $dx_J$  vanishes, then  $(dy, dx_I, d\xi_J)$  are coordinates on  $\Lambda$  nearby,  $I \cup J = \{1, \dots, n\}$ ,  $I \cap J = \{\emptyset\}$ , and one can parameterize  $\Lambda$  as  $\langle X_J(y, x_I, \xi_J) - x_J, \xi_J \rangle$ , where  $x_J = X_J(y, x_I, \xi_J)$  locally on  $\Lambda$  (cf. [18], Thm 21.2.18). The fact that a (possibly empty) set  $I$  exists follows from the canonical graph property, i.e. that  $(y, \eta)$  are local coordinates and  $dy$  linearly independent. Then

$$\begin{aligned} x_{J_i} &= \frac{\partial S_i}{\partial \xi_{J_i}}, & \xi_{I_i} &= -\frac{\partial S_i}{\partial x_{I_i}}, \\ \eta &= \frac{\partial S_i}{\partial y}. \end{aligned} \quad (4)$$

The coordinates are standardly defined on (overlapping) open sets  $O_i$  in  $\Lambda$ , that is,  $(y, x_{I_i}, \xi_{J_i}) \rightarrow r(y, x_{I_i}, \xi_{J_i})$  is defined as a diffeomorphism on  $O_i$ ; let  $i = 1, \dots, N$ . The corresponding partition of unity is written as

$$\sum_{i=1}^N \Gamma_i(r) = 1, \quad r \in \Lambda. \quad (5)$$

In local coordinates, we introduce

$$\bar{\Gamma}_i(y, x_{I_i}, \xi_{J_i}) = \Gamma_i(r(y, x_{I_i}, \xi_{J_i})). \quad (6)$$

Then  $(F\varphi_{\gamma})(y) = \sum_{i=1}^N (F_i\varphi_{\gamma})(y)$  with

$$(F_i\varphi_{\gamma})(y) = \int \int \bar{\Gamma}_i(y, x_{I_i}, \xi_{J_i}) a_i(y, x_{I_i}, \xi_{J_i}) \exp[i \underbrace{(S_i(y, x_{I_i}, \xi_{J_i}) - \langle \xi_{J_i}, x_{J_i} \rangle)}_{\phi(y, x, \xi_{J_i})}] \varphi_{\gamma}(x) dx d\xi_{J_i}. \quad (7)$$

The amplitude  $a_i(y, x_{I_i}, \xi_{J_i})$  is complex and accounts for the KMAH index.

We let  $\Sigma_\phi$  denote the stationary point set (in  $\theta$ ) of  $\phi = \phi(y, x, \theta)$ . The amplitude can be identified with a half-density on  $\Lambda$ . One defines the  $2n$ -form  $d_\phi$  on  $\Sigma_\phi$ ,

$$d_\phi \wedge d \left( \frac{\partial \phi}{\partial \theta_1} \right) \wedge \dots \wedge d \left( \frac{\partial \phi}{\partial \theta_N} \right) = dy_1 \wedge \dots \wedge dy_n \wedge dx_1 \wedge \dots \wedge dx_n \wedge d\theta_1 \wedge \dots \wedge d\theta_N.$$

In the above, we choose  $\lambda = (y, x_I, \frac{\partial \phi}{\partial x_J})$  as local coordinates on  $\Lambda$ , while  $\theta = \xi_J$ . Then we get

$$d_\phi = |\Delta_\phi|^{-1} |d\lambda_1 \wedge \dots \wedge d\lambda_{2n}|, \quad \Delta_\phi = \begin{vmatrix} \frac{\partial^2 \phi}{\partial x_J \partial x_J} & \frac{\partial^2 \phi}{\partial \xi_J \partial x_J} \\ \frac{\partial^2 \phi}{\partial x_J \partial \xi_J} & \frac{\partial^2 \phi}{\partial \xi_J \partial \xi_J} \end{vmatrix} = -1;$$

$\lambda$  is identified with  $(y, x_I, \xi_J)$ . The corresponding half-density equals  $|\Delta_\phi|^{-1/2} |d\lambda_1 \wedge \dots \wedge d\lambda_{2n}|^{1/2}$ .

Densities on a submanifold of the cotangent bundle are associated with the determinant bundle of the cotangent bundle. Let  $a_i^0$  denote the leading order homogeneous part of  $a_i$ . The principal symbol of the Fourier integral operator then defines a half-density,  $a_i^0 d_\phi^{1/2}$ . That is, for a change of local coordinates, if the transformation rule for forms of maximal degree is the multiplication by a Jacobian  $j$ , then the transformation rule for a half-density is the multiplication by  $|j|^{1/2}$ . In our case, of canonical graphs, we can dispose of the description in terms of half-densities and restrict to zero-density amplitudes on  $\Lambda$ .

## 2.2 Propagator

The typical case of a Fourier integral operator associated with a canonical graph is the parametrix for an evolution equation [14, 15],

$$[\partial_t + iP(t, x, D_x)]u(t, x) = 0, \quad u(t_0, x) = \varphi_\gamma(x) \quad (8)$$

on a domain  $X \subset \mathbb{R}^n$  and a time interval  $[t_0, T]$ , where  $P(t, x, D_x)$  is a pseudodifferential operator with symbol in  $S_{1,0}^1$ ; we let  $p$  denote the principal symbol of  $P$ .

For every  $(x, \xi) \in T^*X \setminus \{0\}$ , the integral curves  $(y(x, \xi; t, t_0), \eta(x, \xi; t, t_0))$  of

$$\frac{dy}{dt} = \frac{\partial p(t, y, \eta)}{\partial \eta}, \quad \frac{d\eta}{dt} = -\frac{\partial p(t, y, \eta)}{\partial y}, \quad (9)$$

with initial conditions  $y(x, \xi; t_0, t_0) = x$  and  $\eta(x, \xi; t_0, t_0) = \xi$  define the transformation,  $\chi$ , from  $(x, \xi)$  to  $(y, \eta)$ , which generates the canonical relation of the parameterix of (8), for a given time  $t = T$ ; that is,  $(y(x, \xi), \eta(x, \xi)) = (y(x, \xi; T, t_0), \eta(x, \xi; T, t_0))$ .

The perturbations of  $(y, \eta)$  with respect to initial conditions  $(x, \xi)$  are collected in a propagator matrix,

$$\Pi(x, \xi; t, t_0) = \begin{pmatrix} W_1 & W_2 \\ W_3 & W_4 \end{pmatrix} = \begin{pmatrix} \partial_x y & \partial_\xi y \\ \partial_x \eta & \partial_\xi \eta \end{pmatrix}, \quad (10)$$

which is the solution to the  $2n \times 2n$  system of differential equations

$$\frac{d\Pi}{dt}(x, \xi; t, t_0) = \begin{pmatrix} \frac{\partial^2 p}{\partial \eta \partial y}(t, y, \eta) & \frac{\partial^2 p}{\partial \eta \partial \eta}(t, y, \eta) \\ -\frac{\partial^2 p}{\partial y \partial y}(t, y, \eta) & -\frac{\partial^2 p}{\partial y \partial \eta}(t, y, \eta) \end{pmatrix} \Pi(x, \xi; t, t_0), \quad (11)$$

known as the Hamilton-Jacobi equations, supplemented with the initial conditions [25, 26]

$$\Pi(x, \xi; t_0, t_0) = \begin{pmatrix} \mathbb{I} & 0 \\ 0 & \mathbb{I} \end{pmatrix}. \quad (12)$$

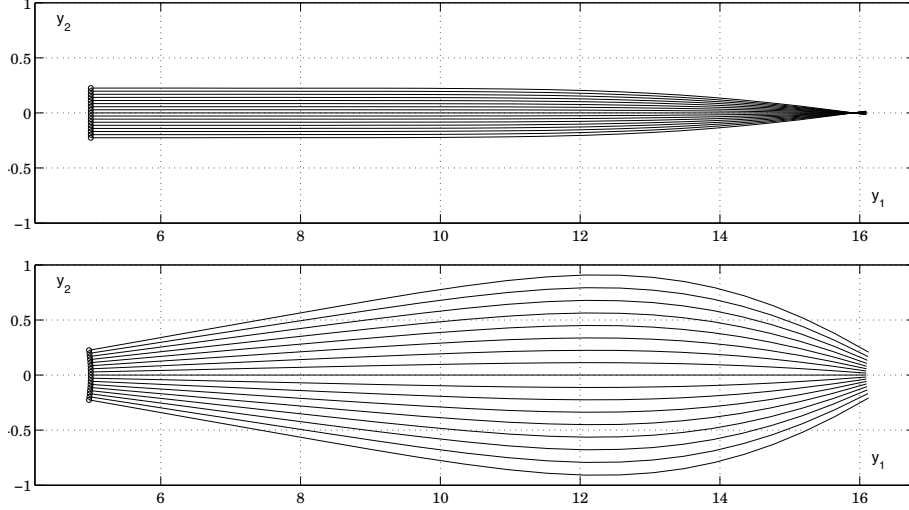


Figure 2: Illustration of canonical relations  $\chi$  (top) and  $\check{\chi}$  (bottom) of operators  $F$  and  $\check{F}$  associated with a half-wave equation: (bi-)characteristics (“rays”) in  $y$  for initial conditions  $(x_2 = x_{2,0}, \xi = \xi_0)$  and  $(\tilde{x}_2 = \tilde{x}_{2,0}, \tilde{\xi} = \tilde{\xi}_0)$ , respectively, for evolution through a low velocity lens (see Section 5). The black circles on the left indicate the conjugate points corresponding to the initial conditions.

Away from caustics the generating function of  $\Lambda$  is  $S = S(y, \xi)$  ( $I_i = \emptyset$ ), which satisfies

$$\frac{\partial^2 S}{\partial y \partial \xi}(y, \xi) = \frac{\partial x}{\partial y} \Big|_{\xi} = W_1^{-1}, \quad (13)$$

$$\frac{\partial^2 S}{\partial \xi^2}(y, \xi) = \frac{\partial x}{\partial \xi} \Big|_y = -\frac{\partial x}{\partial y} \Big|_{\xi} \frac{\partial y}{\partial \xi} \Big|_y = -W_1^{-1} W_2, \quad (14)$$

$$\frac{\partial^2 S}{\partial y^2}(y, \xi) = \frac{\partial \eta}{\partial y} \Big|_{\xi} = \frac{\partial \eta}{\partial x} \Big|_{\xi} \frac{\partial x}{\partial y} \Big|_{\xi} = W_3 W_1^{-1}, \quad (15)$$

upon substituting  $x = x(y, \xi; t_0, T)$  denoting the backward solution to (9) with initial time  $T$ , evaluated at  $t_0$ . The leading-order amplitude follows to be

$$a(y, \xi/|\xi|) = \sqrt{1/\det W_1(x(y, \xi/|\xi|; t_0, T), \xi/|\xi|; T, t_0)}, \quad (16)$$

reflecting that  $a$  is homogeneous of degree 0 in  $\xi$ .

In the vicinity of caustics, we need to choose different coordinates. Admissible coordinates are directly related to the possible rank deficiency of  $W_1$ : One determines the null space of the matrix  $W_1$  and rotates the coordinates such the null space is spanned by the columns indexed by the set  $I_i$ . Then  $(y, x_{I_i}, \xi_{J_i})$  form local coordinates on the canonical relation  $\Lambda$ , as in the previous subsection, and  $O_i$  is given by the set for which the columns indexed by  $I_i$  span the null space of  $W_1$ .

### 3 Singularity resolving diffeomorphisms

We consider the matrix  $W_1(x(y, \xi; t_0, T), \xi; T, t_0)$  for given  $(T, t_0)$  at  $y_0 = y(x_0, \xi_0; T, t_0)$  and  $\xi = \xi_0$  and determine its rank. Suppose it does not have full rank at this point. We construct a diffeomorphism which removes this rank deficiency in a neighborhood of  $r_0 = (y_0, \eta_0; x_0, \xi_0) \in \Lambda$ , where  $\eta_0 = \eta(x_0, \xi_0; T, t_0)$ .

To be specific, we rotate coordinates, such that  $\xi_0 = (1, 0, \dots, 0)$  (upon normalization). Let us assume that the row associated with the coordinate  $x_2$  generates the rank deficiency. (There could be more than one

row / coordinate.) We then introduce the diffeomorphism,

$$Q : x \mapsto \tilde{x} = (x_1 - \frac{\alpha}{2}(x_2 - (x_0)_2)^2, x_2, \dots, x_n);$$

to preserve the symplectic form, we map

$$\xi \mapsto \tilde{\xi} = (\xi_1, \xi_2 + \alpha(x_2 - (x_0)_2) \xi_1, \xi_3, \dots, \xi_n),$$

yielding a canonical transformation  $C_Q : (x, \xi) \mapsto (\tilde{x}, \tilde{\xi})$ . We note that  $C_Q(x_0, \xi_0) = (x_0, \xi_0)$ . The diffeomorphism  $Q$  can be written in the form of an invertible Fourier integral operator with unit amplitude and canonical relation given as the graph of  $C_Q$  (see Appendix A).

The canonical transformation,  $C_Q^{-1}$ , associated with  $Q^{-1}$  is given by

$$\begin{aligned} \tilde{x} \rightarrow x &= (\tilde{x}_1 + \frac{\alpha}{2}(\tilde{x}_2 - x_{0,2})^2, \tilde{x}_2, \dots, \tilde{x}_n), \\ \tilde{\xi} \rightarrow \xi &= (\tilde{\xi}_1, \tilde{\xi}_2 - \alpha(\tilde{x}_2 - x_{0,2}) \tilde{\xi}_1, \dots, \tilde{\xi}_n). \end{aligned}$$

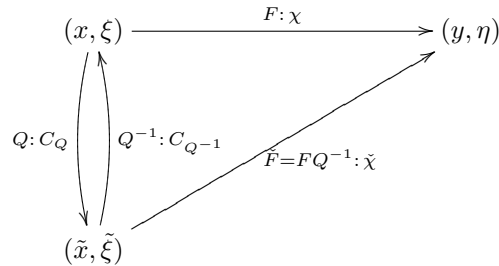
We introduce the pull back,  $Q^*u(\tilde{x}) = u(Q^{-1}(\tilde{x})) = u(\tilde{x}_1 + \frac{\alpha}{2}(\tilde{x}_2 - (x_0)_2)^2, \tilde{x}_2, \dots, \tilde{x}_n)$ . The corresponding propagator matrices are given by

$$\Pi_Q = \begin{pmatrix} \frac{\partial \tilde{x}}{\partial x} & \frac{\partial \tilde{x}}{\partial \xi} \\ \frac{\partial \tilde{\xi}}{\partial x} & \frac{\partial \tilde{\xi}}{\partial \xi} \end{pmatrix} = \begin{pmatrix} 1 & -\alpha(x_2 - x_{0,2}) & 0 & \cdots & 0 & 0 & 0 & \cdots \\ 0 & 1 & 0 & \cdots & 0 & 0 & 0 & \cdots \\ 0 & 0 & 1 & \cdots & 0 & 0 & 0 & \cdots \\ \vdots & \vdots & \vdots & \ddots & \vdots & \vdots & \vdots & \ddots \\ 0 & 0 & 0 & \cdots & 1 & 0 & 0 & \cdots \\ 0 & \alpha \xi_1 & 0 & \cdots & \alpha(x_2 - x_{0,2}) & 1 & 0 & \cdots \\ 0 & 0 & 0 & \cdots & 0 & 0 & 1 & \cdots \\ \vdots & \vdots & \vdots & \ddots & \vdots & \vdots & \vdots & \ddots \end{pmatrix}, \quad (17)$$

$$\Pi_Q^{-1} = \begin{pmatrix} \frac{\partial x}{\partial \tilde{x}} & \frac{\partial x}{\partial \tilde{\xi}} \\ \frac{\partial \xi}{\partial \tilde{x}} & \frac{\partial \xi}{\partial \tilde{\xi}} \end{pmatrix} = \begin{pmatrix} 1 & \alpha(\tilde{x}_2 - x_{0,2}) & 0 & \cdots & 0 & 0 & 0 & \cdots \\ 0 & 1 & 0 & \cdots & 0 & 0 & 0 & \cdots \\ 0 & 0 & 1 & \cdots & 0 & 0 & 0 & \cdots \\ \vdots & \vdots & \vdots & \ddots & \vdots & \vdots & \vdots & \ddots \\ 0 & 0 & 0 & \cdots & 1 & 0 & 0 & \cdots \\ 0 & -\alpha \tilde{\xi}_1 & 0 & \cdots & -\alpha(\tilde{x}_2 - x_{0,2}) & 1 & 0 & \cdots \\ 0 & 0 & 0 & \cdots & 0 & 0 & 1 & \cdots \\ \vdots & \vdots & \vdots & \ddots & \vdots & \vdots & \vdots & \ddots \end{pmatrix}, \quad (18)$$

which are easily verified to be symplectic matrices. In the more general case, each coordinate  $x_j$  generating a rank deficiency yields additional non-zero entry pairs  $\frac{\partial \tilde{x}_1}{\partial x_j}, \frac{\partial x_1}{\partial \tilde{x}_j}, \frac{\partial \tilde{\xi}_j}{\partial x_j}, \frac{\partial \xi_j}{\partial \tilde{x}_j}$ , and  $\frac{\partial \tilde{\xi}_j}{\partial \xi_1}, \frac{\partial \xi_j}{\partial \tilde{\xi}_1}$  in the above

propagator matrices. It follows that the composition  $(\tilde{x}, \tilde{\xi}) \xrightarrow{C_Q^{-1}} (x, \xi) \xrightarrow{\chi} (y, \eta)$  generates the graph of a canonical transformation,  $\tilde{\chi}$  say, which can be parametrized by  $(y, \tilde{\xi})$  locally on an open neighborhood of  $(y_0, \tilde{\xi}(x_0, \xi_0))$ . We denote the corresponding generating function by  $\tilde{S} = \tilde{S}(y, \tilde{\xi})$ . We can compose  $F$  with  $Q^{-1}$  as Fourier integral operators:  $\tilde{F} = FQ^{-1}$ . The canonical relation of  $\tilde{F}$  is the graph of  $\tilde{\chi}$ . In summary:



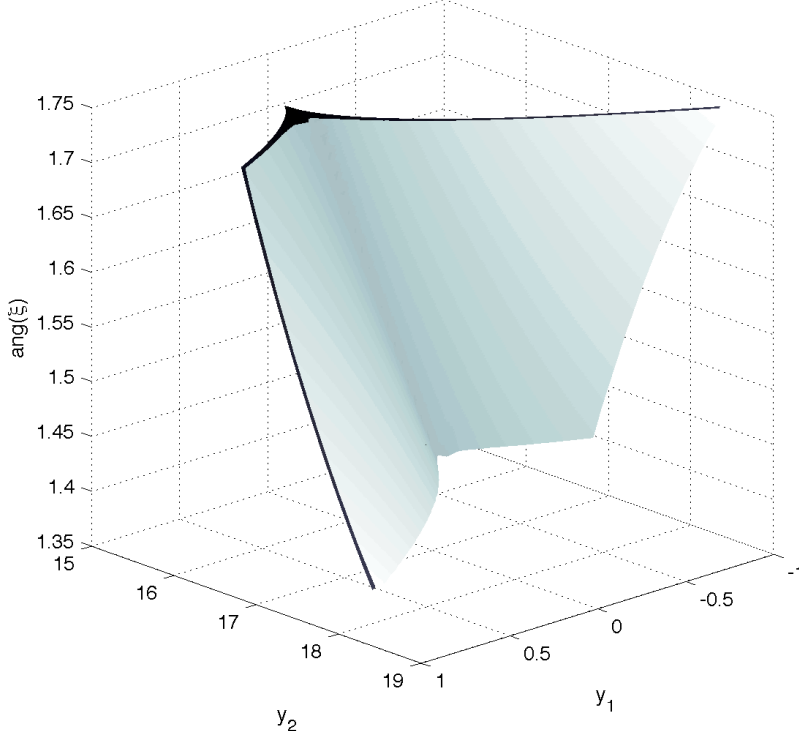


Figure 3: Caustic surfaces  $\Xi(y, \xi)$  (dark gray) and  $\tilde{\Xi}(y, \xi)$  (light gray) of  $\Lambda$  and  $\tilde{\Lambda}$  corresponding to propagation through a low velocity lens (cf. Section 5): The singular regions of  $\Lambda$  and  $\tilde{\Lambda}$  do not intersect.

For each given type of rank deficiency (here, in  $x_2$ ) and each  $(x_0, \xi_0)$  within this class, there is an open set  $O_{(x_0, \xi_0)}$  on which the coordinates  $(I, J)$  are valid. These sets form an open cover, and we obtain a family of diffeomorphisms parametrized by  $(x_0, \xi_0)$ ; there exists a locally finite subcover, and we only need a discrete set to resolve the rank deficiencies everywhere. We index these by  $j = 1, \dots, N_i$  and construct a set of diffeomorphisms,  $\{Q_{ij}\}_{j=1}^{N_i}$ , which resolve locally the rank deficiency leading to coordinates  $(y, x_{I_i}, \xi_{J_i})$ . We write

$$\begin{array}{ccc} (y, x_{I_i}, \xi_{J_i}) & \xrightarrow{\kappa_{ij}} & (y, \tilde{\xi}) \\ \uparrow \downarrow r & & \uparrow \downarrow \tilde{r} \\ \Lambda \ni r = (y, \eta; x, \xi) & \xrightarrow{C_{Q_{ij}}} & (y, \eta; \tilde{x}, \tilde{\xi}) = \tilde{r} \in \tilde{\Lambda}_{ij} \end{array}$$

We write  $\tilde{O}_i$  for the image of  $O_i$  under the diffeomorphism on the level of Lagrangians. Let the matrix  $\frac{\partial^2 \tilde{S}_{ij}}{\partial y \partial \tilde{\xi}}$  in the above be nonsingular on the open set  $\tilde{U}_{ij}$ , and introduce  $\tilde{O}_{ij} = \tilde{U}_{ij} \cap \tilde{O}_i \subset \tilde{\Lambda}_{ij}$ . This set corresponds with a set  $O_{ij} \subset \Lambda$ . We subpartition  $O_i = \cup_{j=1, \dots, N_i} O_{ij}$ . The corresponding partition of unity now reads

$$\sum_{i=1}^N \sum_{j=1}^{N_i} F_{ij}(r) = 1, \quad \text{while } \bar{F}_{ij}(y, x_{I_i}, \xi_{J_i}) = F_{ij}(r(y, x_{I_i}, \xi_{J_i})), \quad j = 1, \dots, N_i. \quad (19)$$

Then  $(F\varphi_\gamma)(y) = \sum_{i=1}^N \sum_{j=1}^{N_i} (F_{ij}\varphi_\gamma)(y)$  with

$$(F_{ij}\varphi_\gamma)(y) = \int \int \bar{F}_{ij}(y, x_{I_i}, \xi_{J_i}) a_i(y, x_{I_i}, \xi_{J_i}) \exp[i(S_i(y, x_{I_i}, \xi_{J_i}) - \langle \xi_{J_i}, x_{J_i} \rangle)] \varphi_\gamma(x) dx d\xi_{J_i}. \quad (20)$$

Inserting the diffeomorphisms, we obtain

$$(F_{ij}\varphi_\gamma)(y) = \int \tilde{A}_{ij}(y, \tilde{\xi}) \exp[i\tilde{S}_{ij}(y, \tilde{\xi})] \widehat{Q_{ij}^* \varphi_\gamma}(\tilde{\xi}) d\tilde{\xi}. \quad (21)$$

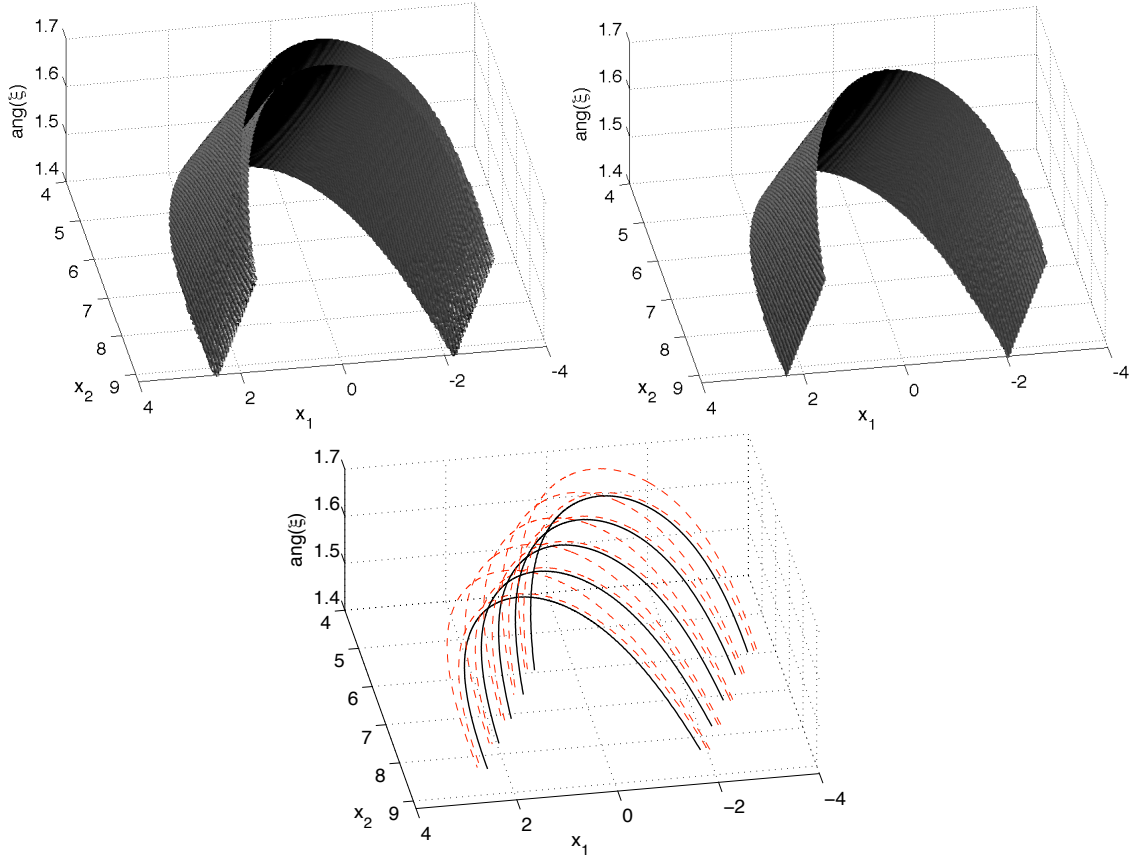


Figure 4: Iso-amplitude surface of the partition functions  $\bar{\Gamma}_i(x, \xi)$ ,  $i = 1, 3$ , associated with  $Q_i = \mathbb{I}$  (left): the joint admissible set  $O_1 \cup O_3$  comprises the exterior of the two sheets. Iso-amplitude surface of  $\bar{\Gamma}_{ij}(x(\tilde{x}, \tilde{\xi}), \xi(\tilde{x}, \tilde{\xi}))$  for  $\xi_0 = \pi/2, x_{2,0} = 0$  and  $\alpha = 1$  ( $i = 2, j = 1$ ) (right): the admissible set  $O_{ij}$  contains the region on the back of the sheet. Bottom: boundaries  $\partial O_i$ ,  $i = 1, 3$  (dashed curves) and  $\partial O_{ij}$ ,  $i = 2, j = 1$  (solid curves) of the admissible domains: Clearly, the joint admissible set  $O_1 \cup O_3 \cup O_{21}$  covers  $\Lambda$ .

The amplitude  $\check{A}_{ij}(y, \tilde{\xi})$  and phase function  $\check{S}_{ij}(y, \tilde{\xi}) - \langle \tilde{\xi}, \tilde{x} \rangle$  are obtained by composing  $F_{ij}$  with  $Q_{ij}^{-1}$  as Fourier integral operators and changing phase variables. It is possible to treat this composition from a semi-group point of view. Then, to leading order, we get

$$\check{A}_{ij}(y, \tilde{\xi}) = \check{\Gamma}_{ij}(y, \tilde{\xi}) \check{a}_{ij}(y, \tilde{\xi}), \quad (22)$$

where

$$\check{\Gamma}_{ij}(y, \tilde{\xi}) = \check{\Gamma}_{ij}(\check{r}(y, \tilde{\xi})), \quad (23)$$

in which

$$\check{\Gamma}_{ij}(\check{r}(r)) = \Gamma_{ij}(r). \quad (24)$$

Moreover,  $\check{a}_{ij}(y, \tilde{\xi})$  can be obtained as follows. If  $\Pi$  is the propagator matrix of the perturbations of  $\chi$ , then the propagator matrix of the perturbations of  $\tilde{\chi}$  is given by:  $\check{\Pi}_{ij} = \Pi \Pi_{Q_{ij}}^{-1}$ . Then

$$\check{a}_{ij}(y, \tilde{\xi}) = \sqrt{1/\det \left( \frac{\partial \check{S}_{ij}(y, \tilde{\xi})}{\partial y \partial \tilde{\xi}} \right)^{-1}}, \quad (25)$$

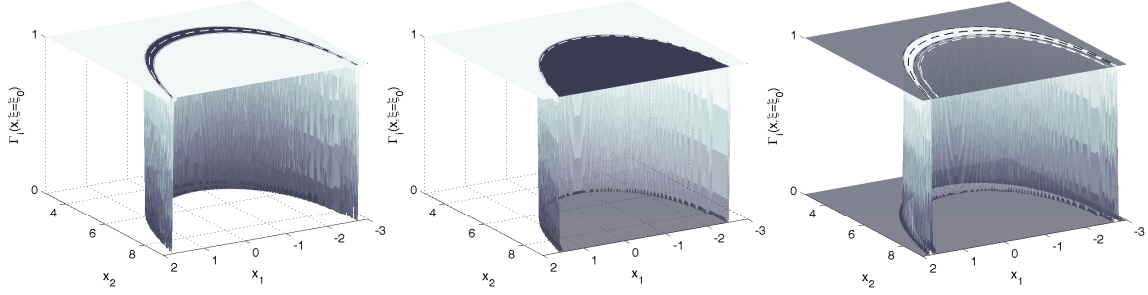


Figure 5: Illustration of joint partition of unity for the partition functions and sets in Fig. 4 for  $\xi_0 = 1.67$  fixed: Slice of  $\bar{\Gamma}_i(x, \xi = \xi_0)$  (left), the admissible set  $U_{ij}$  and the associated partition function  $\bar{\Gamma}_{ij}(x(\tilde{x}, \tilde{\xi}), \xi(\tilde{x}, \tilde{\xi}) = \xi_0)$  (center), and the partition function  $\bar{\Gamma}_{ij}(x(\tilde{x}, \tilde{\xi}), \xi(\tilde{x}, \tilde{\xi}) = 1.67)$  for  $O_{ij}$  realizing the partition of unity with  $\bar{\Gamma}_i(x, \xi = \xi_0)$ .

where  $\det \left( \frac{\partial \check{S}_{ij}(y, \tilde{\xi})}{\partial y \partial \tilde{\xi}} \right)^{-1}$  is obtained as the determinant of the upper-left sub-block of  $\check{\Gamma}_{ij}$ . To accommodate a common notation, we set  $Q_{ij} = \mathbb{I}(N_i = 1)$  if  $I_i = \emptyset$ . In the further analysis, we omit the subscripts  $ij$  where appropriate.

### Expansion of the cutoff functions

The application of our algorithm involves the re-decomposition of  $Q^* \varphi_\gamma$  into wave packets. The key novelty is constructing a separated representation of the partition functions.

Consider our oscillatory integral in  $(y, \tilde{\xi})$  including the cutoff  $\check{I}(y, \tilde{\xi})$ .  $\check{I}(y, \tilde{\xi})$  is homogeneous of degree zero in  $\tilde{\xi}$  and is a classical smooth symbol (of order 0). We “subdivide” the integration over  $\tilde{\xi}$ . A possible procedure involves obtaining a (low-rank) separated representation of  $\check{I}(y, \tilde{\xi})$  on the support of each relevant box in  $\tilde{\xi}$  [3, 5, 4],

$$\check{I}(y, \tilde{\xi}) = \sum_{\beta=1}^{J_{\nu,k}} \check{\Gamma}_1^\beta(y) \check{\Gamma}_2^\beta(\tilde{\xi}), \quad \tilde{\xi} \in B_{\nu,k}. \quad (26)$$

(Basically, this can be obtained using spherical harmonics in view of the fact that the  $\tilde{\xi}$  is implicitly limited to an annulus.) One can view this also as windowing the directions of  $\tilde{\xi}$  into subsets (cones) using  $\check{\Gamma}_2^\beta(\tilde{\xi})$  and then constructing  $\check{\Gamma}_1^\beta(y)$  according to the smallest admissible set in  $y$  for the  $\beta$ -range of directions.

The oscillatory integral becomes

$$(F\varphi_\gamma)(y) = \sum_{\nu,k} \sum_{\beta=1}^{J_{\nu,k}} \check{\Gamma}_1^\beta(y) \int \check{a}(y, \tilde{\nu}) \exp[i\check{S}(y, \tilde{\xi})] \check{\Gamma}_2^\beta(\tilde{\xi}) |\hat{\chi}_{\nu,k}(\tilde{\xi})|^2 \widehat{Q^* \varphi_\gamma}(\tilde{\xi}) d\tilde{\xi}. \quad (27)$$

One can view  $\Gamma_2^\beta(\tilde{\xi}) \hat{\chi}_{\nu,k}(\tilde{\xi})$  as a subdivision of the box  $B_{\nu,k}$ . We know that  $|J_{\nu,k}| \rightarrow 1$  as  $k \rightarrow \infty$  since the cone of directions in  $B_{\nu,k}$  shrinks as  $\sqrt{k}$ . Hence, for large  $k$  this does not involve any action.

The procedure allows a subdivision for coarse scales, as long as the scaling is not affected for large  $k$ . If the subdivision is too “coarse” then parts of the integration will be lost.

## 4 Computation

Here, we develop an algorithm for applying Fourier integral operators in the above constructed universal oscillatory integral representation. The algorithm makes use of the wave-packet based “box-algorithm” computation of the action of Fourier integral operators associated with canonical graphs in microlocal standard

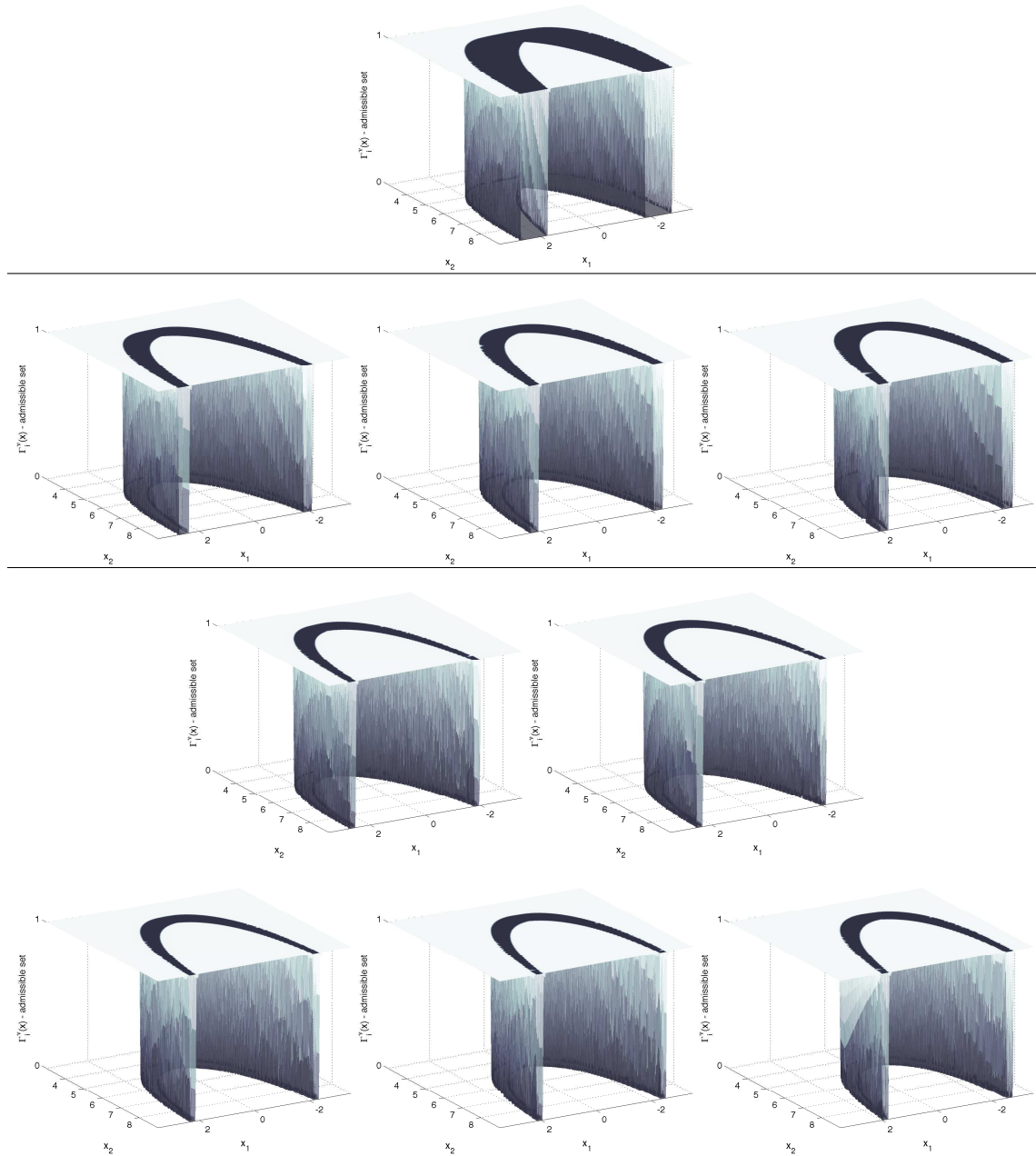


Figure 6: Illustration of admissible sets and expansion functions  $\tilde{\Gamma}_1^\beta(y(x))$  in (26) for the partition functions  $\bar{\Gamma}_i(y(x), \xi)$ ,  $i = 1, 3$ , in Fig. 4:  $J_{\nu,k} = 1$  (top),  $J_{\nu,k} = 3$  (middle), and  $J_{\nu,k} = 5$  (bottom).

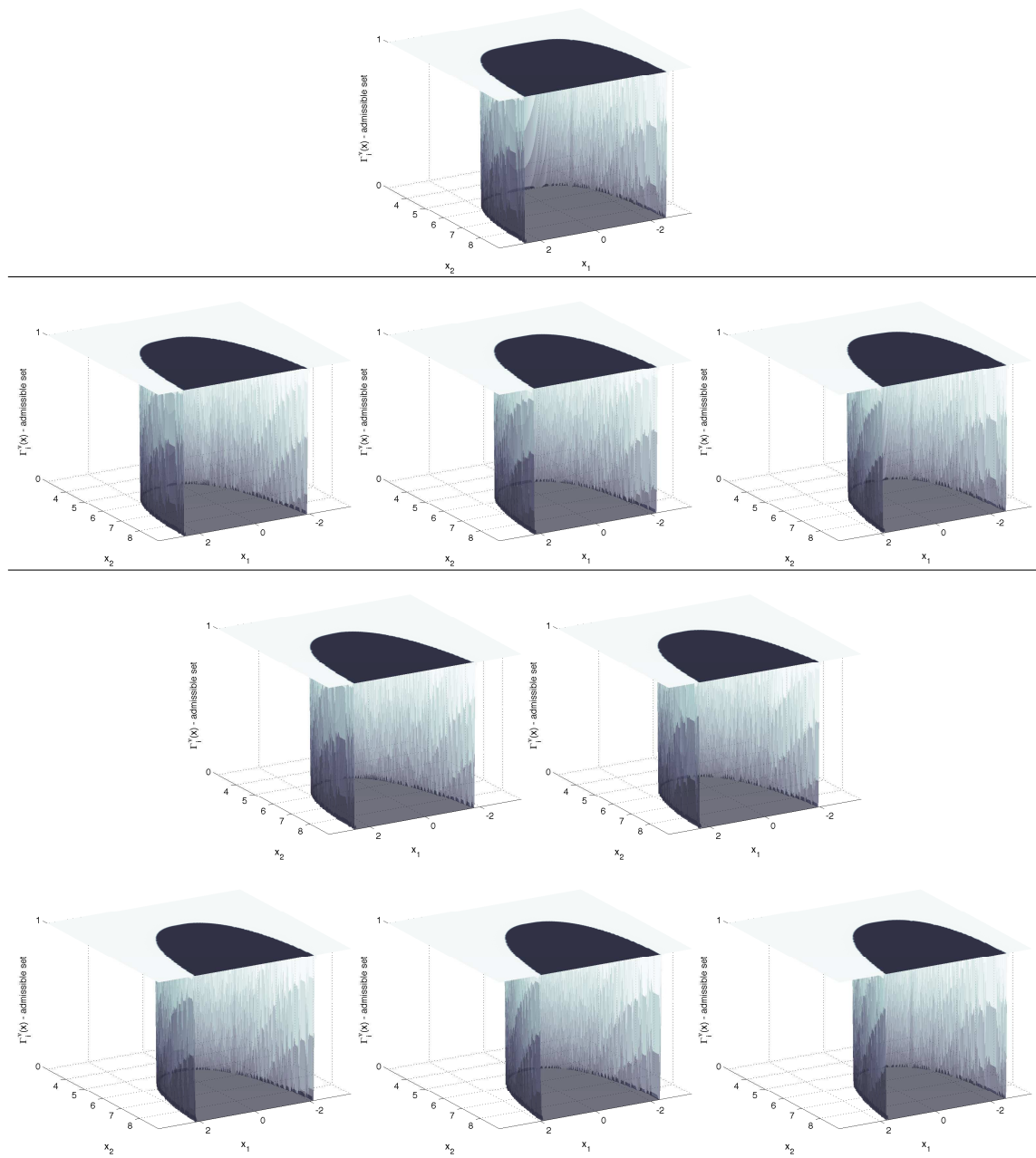


Figure 7: Illustration of admissible sets and expansion functions  $\tilde{\Gamma}_1^\beta(y(x))$  in (26) for the partition functions  $\tilde{\Gamma}_{ij}(y(\tilde{x}, \tilde{\xi}), \xi(\tilde{x}, \tilde{\xi}))$ ,  $i = 2, j = 1$ , in Fig. 4:  $J_{\nu,k} = 1$  (top),  $J_{\nu,k} = 3$  (middle), and  $J_{\nu,k} = 5$  (bottom).

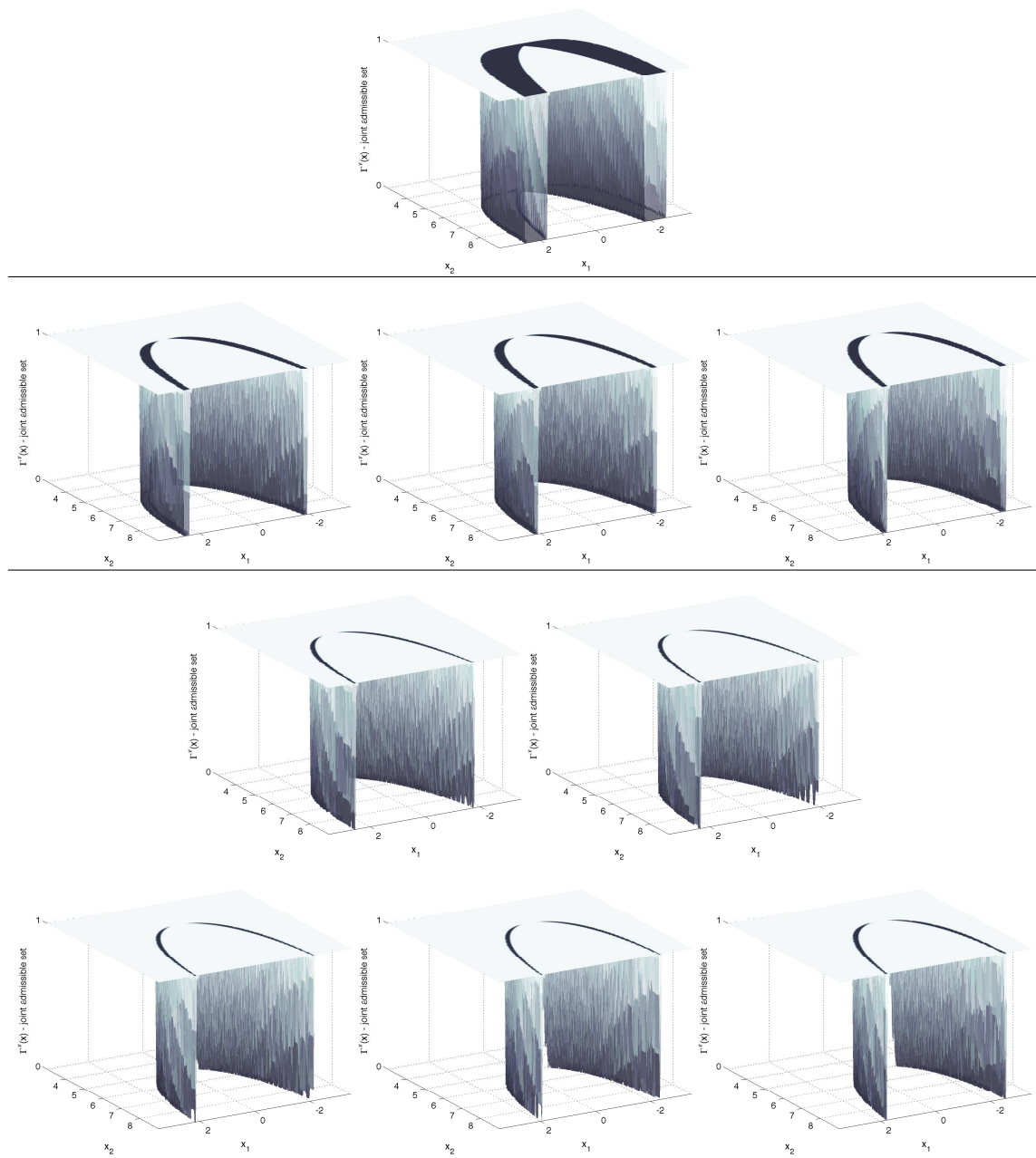


Figure 8: Joint admissible sets and partition of unity for the expansion functions  $\check{\Gamma}_1^\beta(y(x))$  plotted in Fig. 6 and 7:  $J_{\nu,k} = 1$  (top),  $J_{\nu,k} = 3$  (middle), and  $J_{\nu,k} = 5$  (bottom).

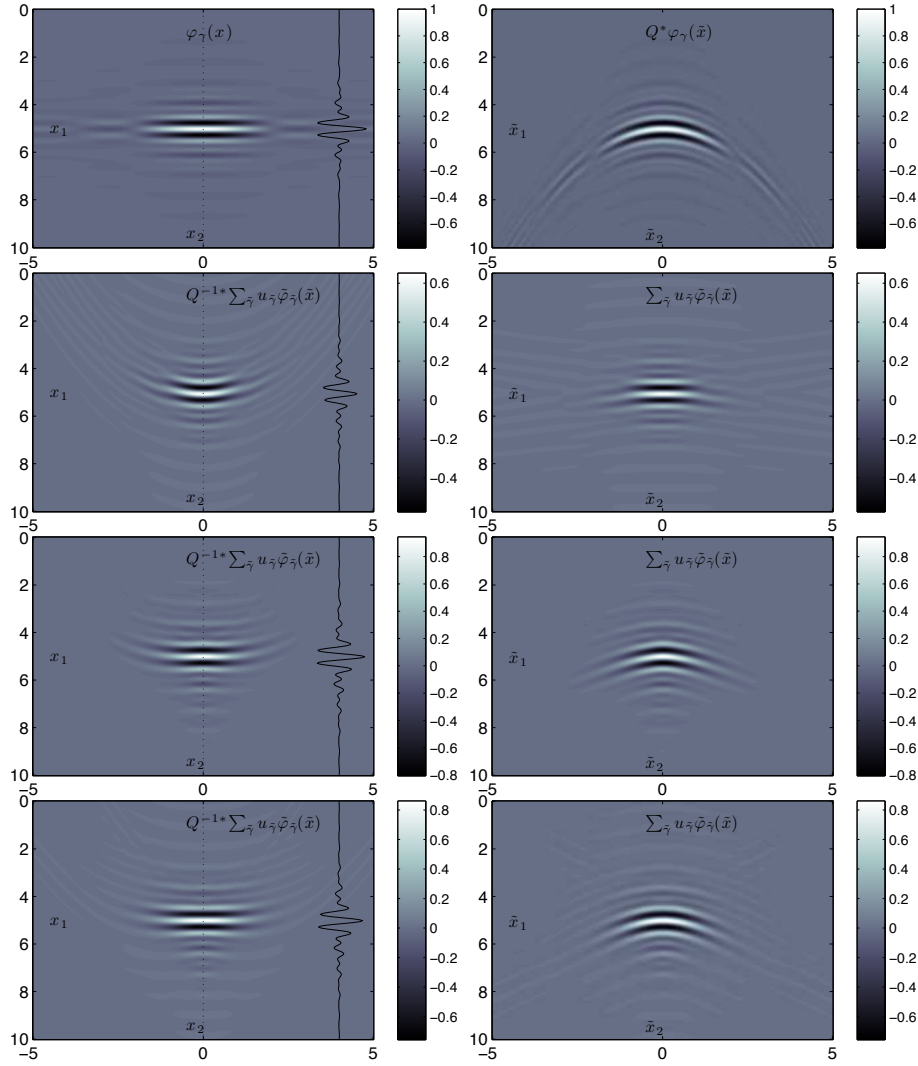


Figure 9: Illustration of diffeomorphism  $Q$ ,  $Q^{-1}$  and re-decomposition for a wave packet  $\varphi_\gamma(x)$  at frequency scale  $k = 2$ . Top row:  $\varphi_\gamma(x)$  (left) and pull-back  $Q^*\varphi_\gamma(\tilde{x})$  (right). Rows 2 to 4: Re-decompositions  $\sum_{\tilde{\nu},k} u_{\tilde{\gamma}} \tilde{\varphi}_{\tilde{\gamma}}(\tilde{x})$  of  $Q^*\varphi_\gamma(\tilde{x})$  using 3, 7, and 9 boxes  $B_{\tilde{\nu},k}$ , respectively (right column), and the corresponding image  $Q^{*-1}\left(\sum_{\tilde{\nu},k} u_{\tilde{\gamma}} \tilde{\varphi}_{\tilde{\gamma}}\right)(x)$  under the action of  $Q^{-1}$  (left column). An insufficient number of boxes alters the amplitudes and the minimum phase property of wave packets. Increasing the number of boxes yields satisfactory results in an open neighborhood of  $(x_0, \xi_0)$ .

focal coordinates  $(y, \tilde{\xi})$  [2]. It is based on the discretization and approximation, to accuracy  $\mathcal{O}(2^{-k/2})$ , of the action of  $\tilde{F}_{ij}$  on a wave packet  $\varphi_{j,\tilde{\nu},k}(\tilde{x})$ ,

$$(\tilde{F}_{ij}\varphi_{\tilde{\gamma}})(y) \approx \check{A}(y, \tilde{\nu}) \sum_{r=1}^R \alpha_{\tilde{\nu},k}^{(r)}(y) \sum_{\tilde{\xi} \in B_{\tilde{\nu},k}} e^{i\langle T_{\tilde{\nu},k}(y), \tilde{\xi} \rangle} |\hat{\chi}_{\tilde{\nu},k}(\tilde{\xi})|^2 \hat{\vartheta}_{\tilde{\nu},k}^{(r)}(\tilde{\xi}). \quad (28)$$

The procedure relies on truncated Taylor series expansions of  $\check{S}_{ij}(y, \tilde{\xi})$  and  $\check{A}(y, \tilde{\xi})$  near the microlocal support of  $\varphi_{\tilde{\gamma}}$ , along the  $\tilde{\nu} = \tilde{\xi}'/|\tilde{\xi}'|$  axis and in the  $\tilde{\xi}''$  directions perpendicular to the radial  $\tilde{\nu} = \tilde{\xi}'$  direction. Here,  $T_{\tilde{\nu},k}(y)$  is the backwards-solution

$$x(y) = T_{\tilde{\nu},k}(y) = \frac{\partial \check{S}_{ij}(y, \tilde{\nu})}{\partial \tilde{\xi}},$$

and  $\alpha_{\tilde{\nu},k}^{(r)}(y)$  and  $\vartheta_{\tilde{\nu},k}^{(r)}(\tilde{\xi})$  are functions realizing, on  $B_{\tilde{\nu},k}$ , a separated tensor-product representation of the slowly oscillating kernel appearing in the second-order expansion term of  $\check{S}_{ij}$ ,

$$\exp \left[ i \frac{1}{2\tilde{\xi}'} \left\langle \tilde{\xi}'', \frac{\partial^2 \check{S}_{ij}}{\partial \tilde{\xi}''^2}(y, \tilde{\nu}) \tilde{\xi}'' \right\rangle \right] B_{\tilde{\nu},k}(\tilde{\xi}) \approx \sum_{r=1}^R \alpha_{\tilde{\nu},k}^{(r)}(y) \vartheta_{\tilde{\nu},k}^{(r)}(\tilde{\xi}). \quad (29)$$

We construct the functions  $\alpha_{\tilde{\nu},k}^{(r)}(y)$  and  $\vartheta_{\tilde{\nu},k}^{(r)}(\tilde{\xi})$  and the tensor product separated representation from prolate spheroidal wave functions [6, 21, 22, 23, 27]. We refer to [2] for a detailed description of the box-algorithm.

## Preparation step

We begin with determining the sets  $O_i$  by computing the perturbations of the integral curves  $(y(x, \xi), \eta(x, \xi))$  with respect to initial conditions  $(x, \xi)$  and monitoring the null space of the matrix  $\frac{\partial y}{\partial x}$ , as detailed in Section 2.2. For parametrices of evolution equations, this involves evaluation of the propagator matrices  $\Pi(x, \xi)$ . Then, for each set  $O_i$ , we detect  $\check{U}_{ij}$  (and consequently  $\check{O}_{ij}$ ) in a similar way, as the sets on which the upper left sub-block of  $\check{\Pi}_{ij} = \Pi \Pi_{Q_{ij}}^{-1}$  has full rank. Here  $\Pi_{Q_{ij}}^{-1}(\tilde{x}, \tilde{\xi})$  is given by (18).

We then proceed with the construction of the partition of unity. Since the partition functions enter the computation as pseudodifferential cutoffs in the construction of the amplitude (cf. (22)), requiring the backwards solutions  $\tilde{x}(y, \tilde{\xi})$  (compare (13–16)), we perform our numerical construction in coordinates  $(\tilde{x}, \tilde{\xi})$ . We obtain  $\check{\Gamma}_{ij}(y, \tilde{\xi})$  upon substituting  $y = y(\tilde{x}, \tilde{\xi})$  implied by the canonical relation  $\check{\chi}_{ij}$ . For the construction of the partition functions  $\check{\Gamma}_{ij}$ , we choose double-exponential cutoffs of the form

$$\exp(-\exp(d(\tilde{x}, \tilde{\xi})))$$

mimicking a  $C_0^\infty$  cutoff, with appropriate normalization and truncated to precision  $\varepsilon$ . Here  $d(\tilde{x}, \tilde{\xi})$  is a function measuring the distance of the point  $(\tilde{x}, \tilde{\xi})$  from the boundary  $\partial \check{U}_{ij}$  of the set  $\check{U}_{ij}(\tilde{x}, \tilde{\xi})$ . The partition of unity is then formed by weighting  $\check{\Gamma}_{ij}(\tilde{x}, \tilde{\xi})$  on the overlaps of the sets  $\check{U}_{ij}(\tilde{x}, \tilde{\xi})$  such that  $\sum_{ij} \check{\Gamma}_{ij}(\tilde{x}, \tilde{\xi}) = 1$ . Finally, we construct the separated representations in  $(\tilde{x}, \tilde{\xi})$  coordinates by windowing the directions of  $\tilde{\xi}$  into subsets using  $\check{\Gamma}_2^\beta(\tilde{\xi})$ , realizing a subdivision into  $\tilde{\xi}$  cones.

## Diffeomorphism

We evaluate  $Q$  in the Fourier domain. The data  $\varphi_\gamma(x)$  enter the box algorithm via the coefficients  $u_\gamma$  of their discrete almost symmetric wave packet transform [13], allowing the fast evaluation of the Fourier transform of the data at a set of frequency points  $\xi_l^{\nu,k}$  limited to the box  $B_{\nu,k}$ . From these, we obtain  $Q_{ij}^* \varphi_\gamma(\tilde{x})$  via evaluation of adjoint unequally spaced FFT [16, 17] at points  $x(\tilde{x})$ .

## Application of the box algorithm

We are now ready to compute the action  $(F_{ij}\varphi_\gamma)(y)$  (cf. (21)) by applying the box algorithm (cf. (28)) to the pull-back  $Q_{ij}^*\varphi_\gamma(\tilde{x})$ . First, we compute the discrete almost symmetric wave packet transform of  $Q_{ij}^*\varphi_\gamma(\tilde{x})$ , yielding its wave packet coefficients  $u_{\mathbb{J},\tilde{\nu},k}$ . Note that numerically significant coefficients  $u_{\mathbb{J},\tilde{\nu},k}$  are contained in a small set of boxes  $B_{\tilde{\nu},k}$  neighboring the direction  $\tilde{\nu} = \xi_0/|\xi_0|$ . We subdivide each box according to the separated representation of  $\tilde{\Gamma}_{ij}$  (cf. (27)). Then, we apply the box algorithm to each subdivision, indexed by triples  $(\beta, \tilde{\nu}, k)$ ,  $\beta = 1, \dots, J_{\tilde{\nu},k}$ . Here, the Taylor series expansion of the generating function  $\tilde{S}_{ij}(y, \tilde{\xi})$  underlying the box algorithm is constructed about the central  $\tilde{\xi}$  direction within the support of  $\Gamma_2^\beta(\tilde{\xi})\hat{\chi}_{\tilde{\nu},k}(\tilde{\xi})$ , accounting for the induced subdivision of the box  $B_{\tilde{\nu},k}$ . Note that sub-dividing into  $\tilde{\xi}$  cones results in a reduction of the range of  $\tilde{\xi}$  orientations in each element  $(\beta, \tilde{\nu}, k)$  of the subdivision, as compared to the  $\tilde{\xi}$  range contained in  $B_{\tilde{\nu},k}$ . This reduces the number  $R$  of expansion terms necessary in the separated tensor product representation for yielding prescribed accuracy, and effectively counter-balances the increase by a factor  $J_{\tilde{\nu},k}$ , evoked by the separated representation of  $\tilde{\Gamma}_{ij}$ , of the number of times the box-algorithm has to be applied.

## Operator hierarchy

The operators  $F_{ij}$  for which  $Q_{ij} = \mathbb{I}$ ,  $F_{ij}^{(\mathbb{I})}$  say, are directly associated with the canonical relation  $\Lambda_F$  and involve only computations on  $\Lambda_F$ . In the algorithm, we reflect this physical hierarchy of the operators  $F_{ij}$  in the construction of the partition of unity. First, we construct a partition of unity for these hierarchically higher operators. Then, we construct a joint partition of the remaining operators on the sets which are not covered by the sets for which  $Q_{ij} = \mathbb{I}$ .

## Re-decomposition

Starting from a single box  $B_{\nu,k}$ , re-decomposition of  $Q^*\varphi_\gamma(\tilde{x})$  results in a set of boxes  $B_{\tilde{\nu},k}$  yielding numerically non-zero contribution to the solution. The number of boxes entering the computation is directly proportional to the computational cost of the algorithm. In applications, we therefore aim at keeping this number small and consider only a subset of boxes, yielding the most significant contributions. We choose this subset such that on an open neighborhood of  $(x_0, \xi_0)$

$$Q_{ij}^{-1}Q_{ij} \approx \mathbb{I}.$$

We can estimate the energy loss induced by the restriction to subsets of  $B_{\tilde{\nu},k}$  and re-normalize the solution. We illustrate the impact of choices of subsets containing different numbers of boxes on the numerical accuracy of the diffeomorphic identity in Fig. 9.

Furthermore, the re-decomposition of  $Q^*\varphi_\gamma(\tilde{x})$  yields in general, under the action of  $Q^{-1}$ ,  $\xi$ -values outside the set  $B_{\nu,k}$ ,  $\xi(x, \tilde{\xi}) \supset B_{\nu,k}$ . We monitor  $\xi(x, \tilde{\xi})$  and do not consider their contribution in our computation if  $|\hat{\chi}_{\nu,k}(\xi(x, \tilde{\xi}))|$  is below a given threshold.

## 5 Numerical example

We numerically illustrate our algorithm for the evaluation of the action of Fourier integral operators associated with evolution equations. We consider wave evolution under the half-wave equation, that is, the initial value problem (8) with symbol

$$P(x, \xi) = \sqrt{c(x)^2 - \|\xi\|^2},$$

in  $n = 2$  dimensions. Here  $c(x)$  stands for the medium velocity.

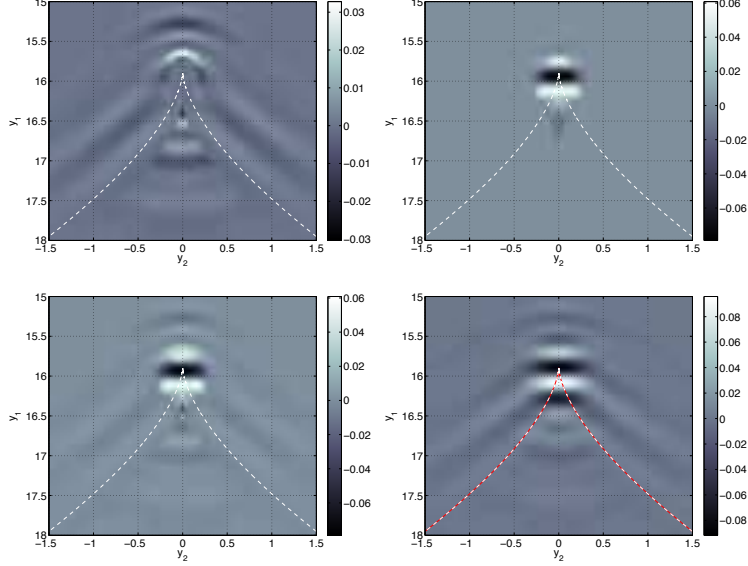


Figure 10: Illustration of operator action on a wave packet  $\varphi_\gamma(x)$  at frequency scale  $k = 2$ : Contribution of operators  $F_i$  ( $i = 1, 3$ ) associated with  $Q_i = \mathbb{I}$  (top left), contribution of operator  $F_{ij}$  ( $i = 2, j = 1$ ) with diffeomorphism parameters  $(\xi_0 = \pi/2, x_{2,0} = 0, \alpha = 1)$ , resolving the singularity in the tip of the caustic (top right), and joint action of  $F_i$  and  $F_{ij}$  (bottom left). Time domain finite difference reference (bottom right). In the operator computation, we consider 9 boxes  $B_{\bar{\nu},k}$  and a separated representation with  $J_{\nu,k} = 1$  term.

## Heterogeneous, isotropic model

We choose a heterogeneous velocity model

$$c(x) = c_0 + \kappa \exp(-|x - x_0|^2/\sigma^2),$$

containing a low velocity lens, with parameters  $c_0 = 2km/s$ ,  $\kappa = -0.4km/s$ ,  $\sigma = 3km$ , and  $x_0 = (0, 14)km$ . As the initial data, we choose horizontal wave packets at frequency scale  $k = 2$  and  $k = 3$ , respectively, in the vicinity of the point  $x' = (0, 5)km$ . We fix the evolution time to  $T = 7s$ . With this choice of parameters, most of the energy of the solution is concentrated near a cusp-type caustic. We illustrate the induced sets  $O_i$  and the joint partition of unity  $\Gamma_i$  in Fig. 4 and 5.

## Operator factorization

We partition the Lagrangian  $\Lambda$  into three sets  $O_i$ ,  $i = \{1, 2, 3\}$ . The sets  $i = \{1, 3\}$  are separated by the caustic. For these sets, we can choose coordinates  $(y, \xi)$ , hence  $Q_i = \mathbb{I}$ . The set  $i = 2$  contains the caustic. For illustration purposes, in the factorization  $F_{ij}$  of  $F_i$  for  $i = 2$ , we choose to compute the operator  $j = 1$ , which resolves the singularity in an open neighborhood of the point indicated by a black dot on the Lagrangian plotted in Fig. 1. This neighborhood contains the cusp of the caustic. Furthermore, we limit our separated representation to one term,  $J_{\nu,k} = 1$  (for the corresponding admissible sets and partition functions, see Fig. 6–8 (top rows)). We restrict the computation of  $F_{ij}$  for the initial data at frequency scale  $k = 2$  ( $k = 3$ ) to 9 (11) boxes  $B_{\bar{\nu},k}$  neighboring the  $\nu$  direction, respectively.

## Results

In Fig. 10, we plot the contributions of the different components in the factorization of the propagator acting on a single horizontal wave packet at frequency scale  $k = 2$ , and compare to a time domain finite difference

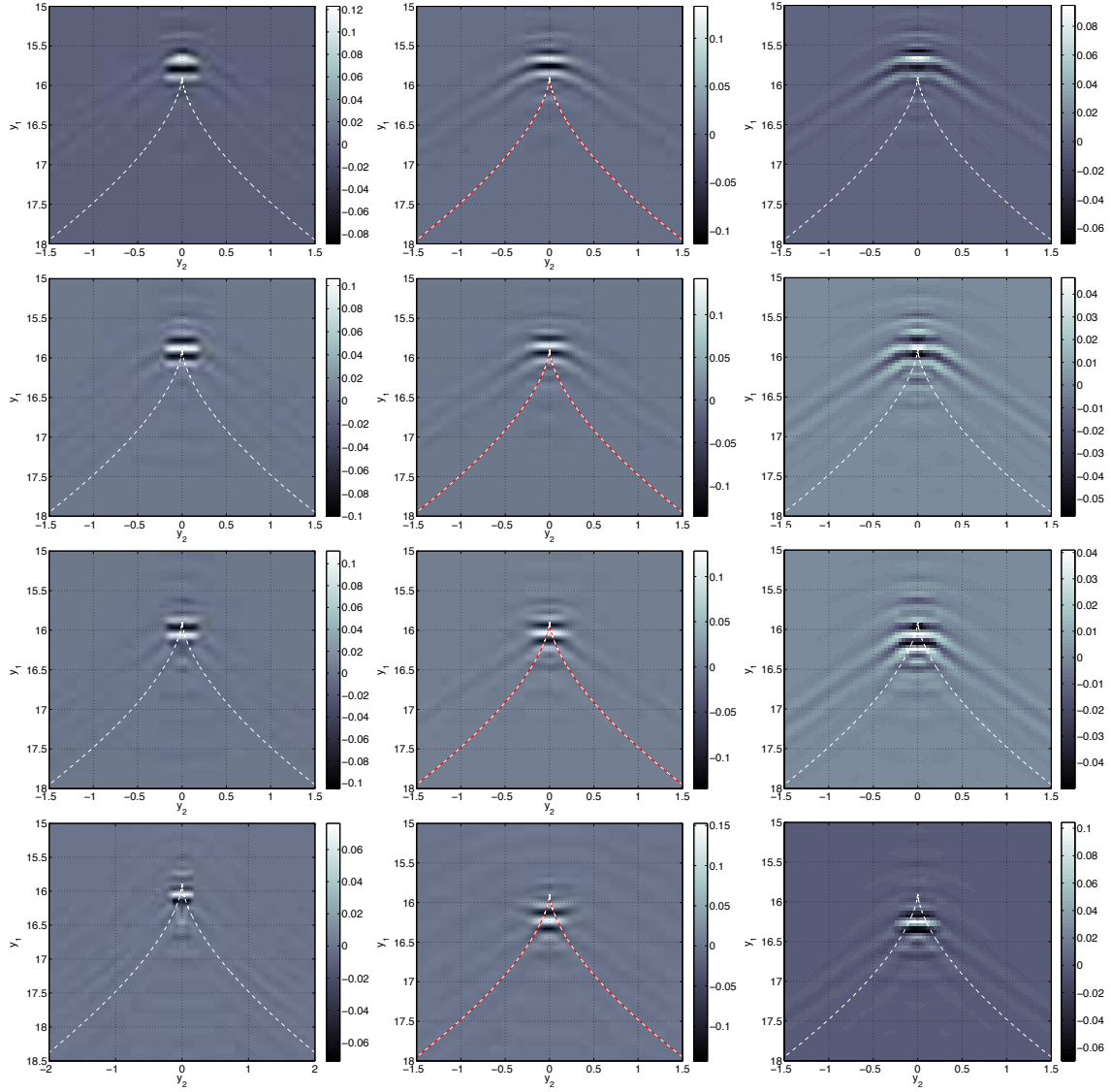


Figure 11: Left column: Joint contribution of the operators  $F_i$  and  $F_{ij}$  acting on a wave packets  $\varphi_\gamma(x)$  at frequency scale  $k = 3$  (compare Fig. 10 (bottom left) for a wave packet at frequency scale  $k = 2$ ). Center column: Time domain finite difference reference. Right column: The equivalent to the left column when using a separated representation with  $J_{\nu,k} = 11$  terms (note that for computational reasons, only 1 box  $B_{\bar{\nu},k}$  has been used in the numerical evaluation of  $F_i$  and  $F_{ij}$  with  $J_{\nu,k} = 11$  terms).

computation. The support of the wave packet within the joint admissible set of the chosen factorization is mostly covered by the set  $O_{ij}$ , such that most of its energy is contributed by the operator  $F_{ij}$ , for which  $Q_{ij} \neq \mathbb{I}$ .

We observe that in the joint admissible set, our algorithm has effectively removed the singularity. We note that the phase of the operator computation matches the phase of the finite difference reference. This includes the KMAH index, which is best observed for operator  $F_3$ , which exclusively contributes to the region beyond the caustic (cf. Fig. 10, top left). Furthermore, note that the amplitude obtained by our algorithm is slightly weaker than the true amplitude. This is consistent with the observations and discussion following Fig. 9 and results from the energy leakage induced by restricting the number of boxes in the re-decomposition step following the application of  $Q$ . We can compensate and re-normalize the amplitude by monitoring the energy loss resulting from the restriction (in Fig. 10, we have not re-normalized the amplitudes). Finally, we note that our algorithm yields the correct result in an open neighborhood in the vicinity of the tip of the caustic, for which we have designed the operator  $F_{ij}$ . In consistency with this fact, it is ineffective for yielding the image of the entire wave packet which, at this low frequency scale, has support extending beyond the admissible set of the operator factors we compute.

These observations are further illustrated in Fig. 11 (left column), where we plot the contributions of the different components in the factorization of the propagator acting on horizontal wave packets, at higher frequency scale  $k = 3$ , centered at locations in the vicinity of the caustic tip (results of a time domain finite difference reference computation are plotted in Fig. 11 (center column)). With these initial data, we explore the open neighborhood about the point for which the operator composition with  $Q_{ij}$  resolves the singularity. Indeed, at this frequency scale, we can obtain the image of an entire wave packet with only one operator factor  $F_{ij}$  (cf. Fig. 11 (second row)). For the wave packet located slightly further above the tip of the caustic (top row), we observe a phase artifact in the region of overlap of  $O_{i=1}$  and  $O_{ij}$ , which can be explained as follows: The restriction of the separated representation for  $F_i$  to one term only induces that the computation of the geometry (bi-characteristics) for the entire box  $B_{\nu,k}$  is exclusively based on one single direction  $\nu$ . This results in inaccuracies in regions close to the caustics where slight perturbations in  $\xi$  yield large variations in  $y$ . Furthermore, as discussed above, wave packets exploring the regions beyond the tip of the caustics eventually start to leave the admissible set for  $F_{ij}$  (third and bottom line).

We note that both for removing the phase artifact of  $F_i$  close to the caustic, and for enlarging the admissible set, it is necessary to increase the number of terms  $J_{\nu,k}$  in the separated representation (26) (compare Fig. 8). This is illustrated in Fig. 11 (right column), where the joint contributions of operators  $F_i$  and  $F_{ij}$  with  $J_{\nu,k} = 11$  terms in the separated representation are plotted. Here, the expansion functions  $\tilde{\Gamma}_2^\beta(\tilde{\xi})$  are constructed as cones in  $\tilde{\xi}$  with a squared cosine cutoff window. For practical reasons and illustration purpose, only one single frequency box  $B_{\tilde{\nu},k}$  has been used in the computation (cf. Fig. 9). While this restriction to only one frequency box affects the amplitudes and the phases in the tails of the wave packet, the separated representation remains nonetheless effective in resolving the issues observed above: the admissible set is extended beyond the caustic and the inaccuracies in the regions of overlap of sets  $O_i$  and  $O_{ij}$  as well as in the regions close to the caustics are considerably reduced.

## 6 Discussion

We developed an algorithm for the evaluation of the action of Fourier integral operators through their factorization into operators with a universal oscillatory integral representation, enabled by the construction of appropriately chosen diffeomorphisms. The algorithm comprises a preparatory geometrical step in which open sets are detected on the canonical relation for which specific focal coordinates are admissible. This covering with open sets induces a pseudodifferential partition of unity. Then, for each term of this partition, we apply a factorization of the associated operators using diffeomorphisms reflecting the rank deficiency and resolving the singularity in the set. This factorization admits a parametrization of the canonical graph in universal  $(y, \tilde{\xi})$  coordinate pairs and enables the application of our previously developed box algorithm, following the dyadic parabolic decomposition of phase space, for numerical computations. Hence, our algorithm enables the discrete wave packet based computation of the action of Fourier integral operators globally,

including in the vicinity of caustics. This wave packet description is valid on the entire canonical relation. It can now enter procedures aiming at the iterative refinement of approximate solutions, and drive the construction of weak solutions via Volterra kernels [1, 12].

In the special case of Fourier integral operators corresponding to parametrices of evolution equations, for isotropic media, an alternative approach for obtaining solutions in the vicinity of caustics has been proposed previously [2, 19, 20]. It consist in a re-decomposition strategy following a multi-product representation of the propagator. Here, we avoid the re-decompositions and operator compositions following the discretization of the evolution parameter, reminiscent of a stepping procedure. What is more, our construction is not restricted to parametrices of evolution equations, but is valid for the general class of Fourier integral operators associated with canonical graphs, allowing for anisotropy. The cost of the algorithm resides in the construction and application of the separated representation of the pseudodifferential partition of unity.

## A Fourier integral representation of $Q$ and $Q^{-1}$

We write  $(Q^*u)(\tilde{x}) = u(X(\tilde{x}))$ ,  $((Q^{-1})^*\tilde{u})(x) = \tilde{u}(\tilde{X}(x))$ . That is,  $X = Q^{-1}$  and  $\tilde{X} = Q$ . The diffeomorphisms  $Q$  and  $Q^{-1}$  define the Fourier integral operators with oscillatory integral kernels,

$$A_Q(\tilde{x}, x) = \int e^{-i\langle \xi, x - X(\tilde{x}) \rangle} d\xi, \quad A_{Q^{-1}}(x, \tilde{x}) = \int e^{-i\langle \tilde{\xi}, \tilde{x} - \tilde{X}(x) \rangle} d\tilde{\xi}. \quad (30)$$

The generating functions are

$$S_Q(\tilde{x}, \xi) = \langle \xi, X(\tilde{x}) \rangle, \quad S_{Q^{-1}}(x, \tilde{\xi}) = \langle \tilde{\xi}, \tilde{X}(x) \rangle,$$

respectively. The canonical relations are the graphs of  $C_Q$  and  $C_{Q^{-1}}$ , and are given by

$$\Lambda_Q = \{(\tilde{x} = X^{-1}(x), \langle \xi, \partial_{\tilde{x}} X \rangle|_{\tilde{x}=X^{-1}(x)}; x, \xi)\}, \quad \Lambda_{Q^{-1}} = \{(x = \tilde{X}^{-1}(\tilde{x}), \langle \tilde{\xi}, \partial_x \tilde{X} \rangle|_{x=\tilde{X}^{-1}(\tilde{x})}; \tilde{x}, \tilde{\xi})\}.$$

The Hessians yield a unit amplitude:

$$\left| \det \frac{\partial^2 \langle \xi, X(\tilde{x}) \rangle}{\partial \tilde{x} \partial \xi} \right| = 1, \quad \left| \det \frac{\partial^2 \langle \tilde{\xi}, \tilde{X}(x) \rangle}{\partial x \partial \tilde{\xi}} \right| = 1.$$

Substituting the particular diffeomorphism, we obtain:

$$\begin{aligned} \partial_x \tilde{X}|_{x=\tilde{X}^{-1}(\tilde{x})} &= \begin{pmatrix} 1 & -\alpha(\tilde{x}_2 - x_{0,2}) & 0 & \cdots \\ 0 & 1 & 0 & \cdots \\ 0 & 0 & 1 & \cdots \\ \vdots & \vdots & \vdots & \ddots \end{pmatrix} \\ \langle \tilde{\xi}, \partial_x \tilde{X} \rangle|_{x=\tilde{X}^{-1}(\tilde{x})} &= \begin{pmatrix} \tilde{\xi}_1 \\ \tilde{\xi}_2 - \alpha(\tilde{x}_2 - x_{0,2})\tilde{\xi}_1 \\ \vdots \end{pmatrix}. \end{aligned}$$

## References

- [1] F. Andersson, M. V. de Hoop, H.F. Smith, and G. Uhlmann. A multi-scale approach to hyperbolic evolution equations with limited smoothness. *Comm. Partial Differential Equations*, 33:988–1017, 2008.
- [2] F. Andersson, M.V. de Hoop, and H. Wendt. Multi-scale discrete approximation of Fourier integral operators. *SIAM Multiscale Model. Simul.*, 10:111–145, 2012.

- [3] G. Bao and W.W. Symes. Computation of pseudodifferential operators. *SIAM J. Sci. Comput.*, 17:416–429, 1996.
- [4] G. Beylkin, V. Cheruvu, and F. Pérez. Fast adaptive algorithms in the non-standard form for multidimensional problems. *Appl. Comput. Harmon. Anal.*, 24:354–377, 2008.
- [5] G. Beylkin and M.J. Mohlenkamp. Algorithms for numerical analysis in high dimensions. *SIAM J. Sci. Comput.*, 26(6):2133–2159, 2005.
- [6] G. Beylkin and K. Sandberg. Wave propagation using bases for bandlimited functions. *Wave Motion*, 41:263–291, 2005.
- [7] B. Bradie, R. Coifman, and A. Grossmann. Fast numerical computations of oscillatory integrals related to acoustic scattering, i. *Appl. Comput. Harmon. Anal.*, 1(1):94–99, 1993.
- [8] E. Candès and L. Demanet. Curvelets and Fourier integral operators. *C. R. Acad. Sci. Paris*, I(336):395–398, 2003.
- [9] E. Candès, L. Demanet, D. Donoho, and L. Ying. Fast discrete curvelet transforms. *SIAM Multiscale Model. Simul.*, 5(3):861–899, 2006.
- [10] E. Candès, L. Demanet, and L. Ying. Fast computation of Fourier integral operators. *SIAM J. Sci. Comput.*, 29(6):2464–2493, 2007.
- [11] E. Candès, L. Demanet, and L. Ying. A fast butterfly algorithm for the computation of Fourier integral operators. *SIAM Multiscale Model. Simul.*, 7:1727–1750, 2009.
- [12] M.V. de Hoop, S.F. Holman, H.F. Smith, and G. Uhlmann. Regularity and multi-scale discretization of the solution construction of hyperbolic evolution equations with limited smoothness. *Appl. Comput. Harmon. Anal.*, 33:330–353, 2012.
- [13] A. Duchkov, F. Andersson, and M.V. de Hoop. Discrete almost symmetric wave packets and multi-scale representation of (seismic) waves. *IEEE T. Geosci. Remote Sensing*, 48(9):3408–3423, 2010.
- [14] A. Duchkov and M.V. de Hoop. Extended isochron rays in shot-geophone (map) migration. *Geophysics*, 75(4):139–150, 2010.
- [15] A. Duchkov, M.V. de Hoop, and A. Sá Baretto. Evolution-equation approach to seismic image, and data, continuation. *Wave Motion*, 45:952–969, 2008.
- [16] A. Dutt and V. Rokhlin. Fast Fourier transforms for nonequispaced data. *SIAM J. Sci. Comput.*, 14(6):1368–1393, 1993.
- [17] A. Dutt and V. Rokhlin. Fast Fourier transforms for nonequispaced data II. *Appl. Comput. Harmon. Anal.*, 2:85–100, 1995.
- [18] L. Hörmander. *The Analysis of Linear partial Differential Operators*, volume IV. Springer-Verlag, Berlin, 1985.
- [19] H. Kumano-go, K. Taniguchi, and Y. Tozaki. Multi-products of phase functions for Fourier integral operators with an applications. *Comm. Partial Differential Equations*, 3(4):349–380, 1978.
- [20] J.H. Le Rousseau. Fourier-integral-operator approximation of solutions to first-order hyperbolic pseudodifferential equations i: convergence in Sobolev spaces. *Comm. PDE*, 31:867–906, 2006.
- [21] D. Slepian. Prolate spheroidal wave functions, Fourier analysis and uncertainty–IV: extensions to many dimensions, generalized prolate spheroidal wave functions. *Bell Syst. Tech. J.*, November:3009–3057, 1964.

- [22] D. Slepian. On the symmetrized Kronecker power of a matrix and extensions of Mehler's formula for Hermite polynomials. *SIAM J. Math. Anal.*, 3:606–616, 1972.
- [23] D. Slepian. Prolate spheroidal wave functions, Fourier analysis and uncertainty–V: the discrete case. *Bell Syst. Tech. J.*, 57:1371–1430, 1978.
- [24] H. Smith. A parametrix construction for wave equations with  $C^{1,1}$  coefficients. *Ann. Inst. Fourier, Grenoble*, 48:797–835, 1998.
- [25] V. Červený. *Seismic ray theory*. Cambridge University Press, Cambridge, UK, 2001.
- [26] V. Červený. A note on dynamic ray tracing in ray-centered coordinates in anisotropic inhomogeneous media. *Stud. Geophys. Geod.*, 51:411–422, 2007.
- [27] H. Xiao, V. Rokhlin, and N. Yarvin. Prolate spheroidal wave functions, quadrature and interpolation. *Inverse problems*, 17:805–838, 2001.